



RESEARCH ARTICLE

^{10}Be exposure age for sorted polygons in the Sudetes Mountains

Zbyněk Engel¹  | Marek Křížek¹ | Régis Braucher² | Tomáš Uxa^{1,3}  | David Krause^{1,4} | AsterTeam²

¹Department of Physical Geography and Geoecology, Faculty of Science, Charles University, Prague, Czech Republic

²Collège de France, CEREGE CNRS Aix Marseille Université, IRD, INRAE, Aix-en-Provence, France

³Department of Geothermics, Institute of Geophysics, Academy of Sciences of the Czech Republic, Prague, Czech Republic

⁴The Krkonoše Mountains National Park Administration, Vrchlabí, Czech Republic

Correspondence

Zbyněk Engel, Department of Physical Geography and Geoecology, Faculty of Science, Charles University, Prague, Czech Republic.
Email: engel@natur.cuni.cz

Funding information

The Czech Science Foundation, Grant/Award Number: 17-21612S

Abstract

Patterned-ground landforms represent the most common phenomenon of periglacial environment, and their large sorted forms belong to the few morphological indicators of past permafrost distribution. The relic forms of patterned ground are widespread on high-elevated surfaces in the central European uplands, providing the evidence of regional periglacial conditions in the last glacial period. However, the timing of these landforms, as well as their potential for paleoclimate reconstructions, has remained unexplored. In this paper, we present ^{10}Be exposure ages from the large sorted polygons sampled at four sites in the Sudetes Mountains, the highest part of the central European uplands. These results indicate that these landforms started to form at the end of Marine Isotope Stage 3, and the main phase of their formation occurred between 30 and 20 ka. This research confirms the hypothesis of sorted patterned-ground formation within the last (Weichselian) glacial stage (110.6–11.7 ka) and suggests that earlier-sorted features are not preserved in the Sudetes. The recognized period of enhanced periglacial activity coincides with a prominent cold interval identified earlier in both regional and northern-hemispheric proxy records.

KEYWORDS

Central Europe, cosmogenic-nuclide dating, past permafrost, patterned ground, periglacial environment, Quaternary

1 | INTRODUCTION

Cryogenic sorted patterned ground refers to the arrangement of segregated fine and coarse materials that form at the ground surface as a result of differential frost heave and soil circulation.¹ The resulting forms are more or less symmetric features among which circles and polygons are most common. The polygonal pattern reflects the uneven penetration of freezing planes into the ground, displacement of clasts from concentrations of finer soil toward pattern margins, and lateral interaction of adjacent fine cells.² Small-scaled circles and polygons (<1 m in diameter) form in seasonally frozen ground, but larger sorted forms are found only in areas underlain by permafrost.³ Relict

large sorted polygons thus provide evidence for the former existence of permafrost and indicate paleoclimatic conditions.⁴

The distribution of cryogenic sorted patterned ground has been frequently used for spatial reconstructions of periglacial environment during the cold stages of the Quaternary as their distinct pattern can be easily identified in the field and remotely sensed data. Moreover, dimensions of large (>1 m wide) sorted patterned ground indicate the thickness of the former active layer that corresponds to the depth of sorting and landform width.⁵ The paleoclimatic interpretation of patterned ground has been mostly considered limited because of the complex history of its formation and the possible influence of non-climate-related local factors.⁶ However, large sorted polygons indicate the lack of a thick snow cover, frequent freeze–thaw cycles in the active layers, and air temperature thresholds required for differential sorting and frost

AsterTeam: Georges Aumaitre, Didier Bourlès, Karim Keddadouche

heave.⁷ Now, large sorted patterns are active in the permafrost areas with mean annual air temperature (MAAT) lower than -6 to -3°C .^{8,9} Therefore, these landforms can, when constrained by geochronological data, provide insights into Quaternary climatic conditions.

Unfortunately, there is still no robust approach for the dating of patterned ground despite the recent advances in geochronology. The main problem for dating these structures results from the complex history of their formation as they can develop over a short/long time span and/or during multiple cold events.¹⁰ Large sorted polygons are products of recurrent freezing and thawing of the active layer, which causes upward movements of coarse clasts from the permafrost table and their subsequent migration toward the margins of the polygons.^{11,12} Under prolonged freeze–thaw conditions, the boulders forming the margins may be tilted due to the lateral squeezing of the adjacent polygons.¹³ Although this process can decrease the exposure age of the boulders, it probably affects the minor parts of clasts. If the frequency of freeze–thaw cycles drops back to the non-permafrost conditions, the supply of clasts via frost heave and lateral sorting ceases, and large boulders at the margin of the polygons stabilize, attesting to the last time of their activity. Smaller patterns may eventually form in the center of the inactive polygons at a later time if environmental conditions become suitable.³

Since the 1990s, radiocarbon, luminescence, and *in situ*-produced cosmogenic nuclides (TCN) dating methods have been applied on patterned-ground forms to determine their ages. Radiocarbon ages were reported mostly for non-sorted patterned ground, especially earth hummocks, rich in organics.¹⁴ Only a small amount of radiocarbon data was obtained for sorted patterned ground^{15–17} that usually contains a small amount of organic material. Moreover, this material may have formed earlier or later than the landform itself.¹⁶ Thermoluminescence and optically stimulated luminescence dating have been used for the dating of non-sorted circles, stripes, and polygons,^{18–20} but a successful application remains challenging.²¹ Apart from the issues related to the polycyclic nature of these features,¹⁹ the possible incorporation of incompletely bleached grains and fluctuations of the water content after sedimentation of the material complicate the interpretation of the luminescence data.²² The application of TCN in the dating of patterned ground is still rare. The method has been used only to estimate the timing of poorly sorted patterns based on the dating of underlying rock glaciers^{23,24} and to obtain Schmidt-hammer exposure ages for sorted circles and stripes.^{6,25} The most frequent applications of TCN in the periglacial landscape include the determination of “periglacial trimlines”²⁶ and the timing of rock glaciers²⁷ and boulder fields.²⁸

This paper aims at constraining the timing of sorted polygons in the Sudetes Mountains, the highest section of the central European uplands. This region is characterized by large surfaces of low relief above 1,200 m a.s.l. (referred to as summit planation surfaces in this paper)²⁹ with well-developed periglacial landforms. Among these landforms, sorted patterned-ground phenomena were recognized first because of their distinctive morphology and widespread distribution.³⁰ An earlier hypothesis relates their origin to past glacial cycles and attributes most of the preserved forms to the culmination phase of the last glacial period.³¹ An alternative view suggests that most

sorted patterned ground in the Sudetes Mountains formed during the late glacial period.³² In either case, the chronology of these landforms and paleoclimatic conditions during the period of their formation remain uncertain. To constrain the timing of the formation of large sorted polygons and to infer the paleoclimatic conditions for this period, we analyzed their distribution and morphology in the Krkonoše and Hrubý Jeseník Mountains, the highest parts of the Sudetes. Twenty-four new ^{10}Be surface exposure ages from four sorted polygon assemblages were produced, and the established chronology was compared with a local set of exposure ages reported for glacial and periglacial landforms and with the existing records of paleoenvironmental conditions in Central Europe.

2 | STUDY AREA

The Sudetes Mountains on the Czech–Polish boundary represent a 340-km-long eastern section of the central European uplands that stretch along 50°N . During the Quaternary glaciations, the Sudetes Mountains were located within the periglacial zone between the Fennoscandian ice sheet and ice cap over the Alps (Figure 1, inset). The width of the zone ranged from 430 km in the Last Glacial Maximum (LGM) to more than 1,300 km during the Middle Weichselian interstadial. The periglacial processes throughout this area and loess deposition in the lowlands dominated the development of this zone over cold stadial episodes. An extensive loess deposition belt formed in the northern part of the zone, whereas a more-scattered loess cover formed at the southern front of the Sudetes Mountains below 450 m a.s.l.³³ Periglacial processes have been most intense on summit planation surfaces where the annual precipitation was estimated to range from 500 to 700 mm during the LGM³⁴ and the temperature depression ranged from 7 to 10°C .³⁵ During the last glaciation, cirque and valley glaciers modified the central part of the ranges,³⁶ but periglacial landscape prevailed in the Sudetes Mountains.

The Sudetes Mountains are located in a transitional zone between areas dominated by the oceanic climate and the continental-type regimes. The precipitation on summit planation surfaces decreases from the Krkonoše Mountains in the western part of the Sudetes Mountains ($>1,500$ mm per year)³⁹ to the Hrubý Jeseník Mountains near the eastern margin of the range (1,200–1,300 mm per year).⁴⁰ The MAAT for the period 1961–1990 ranged from 0.4°C at the Sněžka weather station (1,603 m a.s.l.) in the Krkonoše Mountains to 0.9°C at the Praděd station (1,492 m a.s.l.) in the Hrubý Jeseník Mountains to $\sim 3^{\circ}\text{C}$ at an elevation of 1,200 m a.s.l.⁴¹ Westerly winds prevail within the Sudetes Mountains transporting snow from the summit plateaus to leeward slopes.⁴²

The Krkonoše Mountains comprise a west northwest-east southeast-oriented main (Silesian) ridge built of mid-Carboniferous granites (~ 320 – 315 Ma) and a parallel southern (Bohemian) ridge at the contact between the plutonic complex and Neoproterozoic to Lower Paleozoic metamorphic rocks.⁴³ The ridges delimit the relics of high-elevated (1,350–1,500 m a.s.l.)⁴⁴ planation surfaces (Figures 1a and 2a) formed as a result of slow weathering and

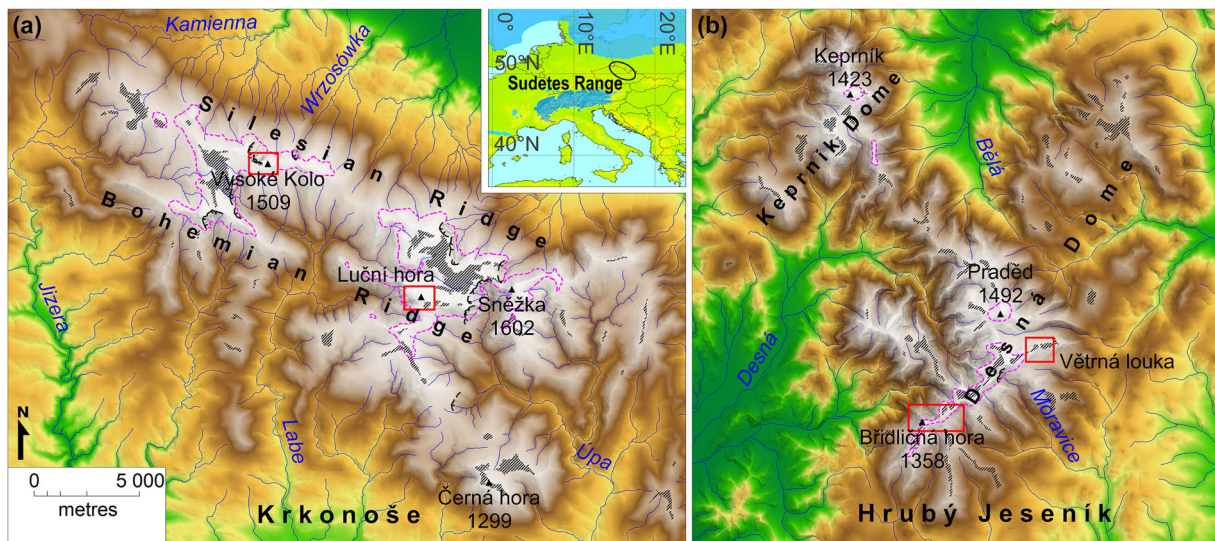


FIGURE 1 Location of the study sites (red boxes) in the (a) Krkonoše and (b) Hrubý Jeseník Mountains and their position in the Sudetes Range (black ellipse) in Central Europe (inset map). Oblique hatching marks planation surfaces and thick black lines indicate glacial cirques. Dashed purple line indicates the alpine timberline,³⁷ and blue shades in the inset map show the Last Glacial Maximum extent of glaciers³⁸

long-term denudation that probably started ~ 75 Ma.⁴⁵ The Hrubý Jeseník Mountains consist of Keprník and Desná Domes oriented approximately northeast–southwest (Figure 1b). Both domes are built by a Cadomian crystalline basement imbricated with metamorphosed Devonian volcanosedimentary complexes.⁴⁶ The domes have well-developed summit planation surfaces at 1,300–1,460 m a.s.l.,⁴⁷ which are more extensive in the southern part of the Desná Dome (Figure 3a). The planation surfaces in both the Krkonoše and Hrubý Jeseník Mountains are covered with thin weathering mantle and periglacial features among which relic sorted polygons and nets prevail.⁴⁸

The four studied sites are located in high-elevated parts of the Sudetes Mountains. Vysoké Kolo (VK, 1,509 m a.s.l.), the highest granite elevation in the western Krkonoše Mountains, and quartzite-dominated Luční hora (LH, 1,555 m a.s.l.) on the Bohemian ridge (Figure 1a) represent the highest summit planation surfaces in the Sudetes Mountains. Břidličná hora (BR, 1,358 m a.s.l.) and Větrná louka (VL, 1,250–1,270 m a.s.l.) consist of phyllites and represent the southern part of the Hrubý Jeseník Mountains (Figure 1b). BR belongs to the highest elevation on the Desná Dome, whereas VL is located on a lowered planation surface on a side ridge (Figure 3). Products of *in situ* weathering dominate at all sites, and small sections of exposed bedrock are present only on LH. All sites except VL are located in the zone of limited vegetation above the timberline (Figures 1 and 3e).

3 | METHODS

3.1 | Morphological analyses and boulder sampling

We selected four study sites with the best-developed and undisturbed sorted polygons in the Sudetes Mountains for

morphological analyses and ¹⁰Be sampling. The length, width, and height of the 81 sorted polygons were measured at these sites. The height is defined as the maximum vertical distance between the lowest point at the polygon border and the highest point at its updomed center.⁴⁹ Between-site differences in the height and width of the sorted polygons were assessed using a one-way analysis of variance (ANOVA) and tested using an *F*-test at the significance level $p = 0.05$. The length of the sorted polygons was excluded from the ANOVA analyses because this parameter can relate to the surface inclination and thus it can reflect other factors, such as solifluction.⁵⁰ The width of the polygons was used to estimate the thickness of the past active layer based on the regression equation (Figure 4) for a set of published paired data.^{4,5,9,51–67}

The sorting depth for polygons and the thickness of weathered rocks at study sites were determined using electrical resistivity tomography. Soundings were carried out across the given polygon assemblage between the nearest edges of the given summit flat. The method was applied at multiple four-electrode arrays with 2-m spacing between the electrodes using the Wenner-Schlumberger measuring method.⁶⁸ The obtained apparent resistivity data were subjected to the geophysical inversion procedure (L1-norm) using RES2DINV software (Geotomo, Gelugor, Malaysia).

We sampled six boulders per site to increase the possibility of deriving a robust ¹⁰Be chronology. At each site, we collected samples from two to three individual sorted polygons. The samples were collected preferentially from the largest upright boulders located at the border of a sampled undisturbed polygon. This approach limits the possibility of the tilting of boulders after their active upfreezing/frost heaving and reduces the effects of snow and vegetation cover.⁶⁹ The samples were collected using a chisel and a hammer; the samples were taken from the sampled surface to a depth of 2–7 cm. The dip/orientation of the sampled surfaces was measured using a

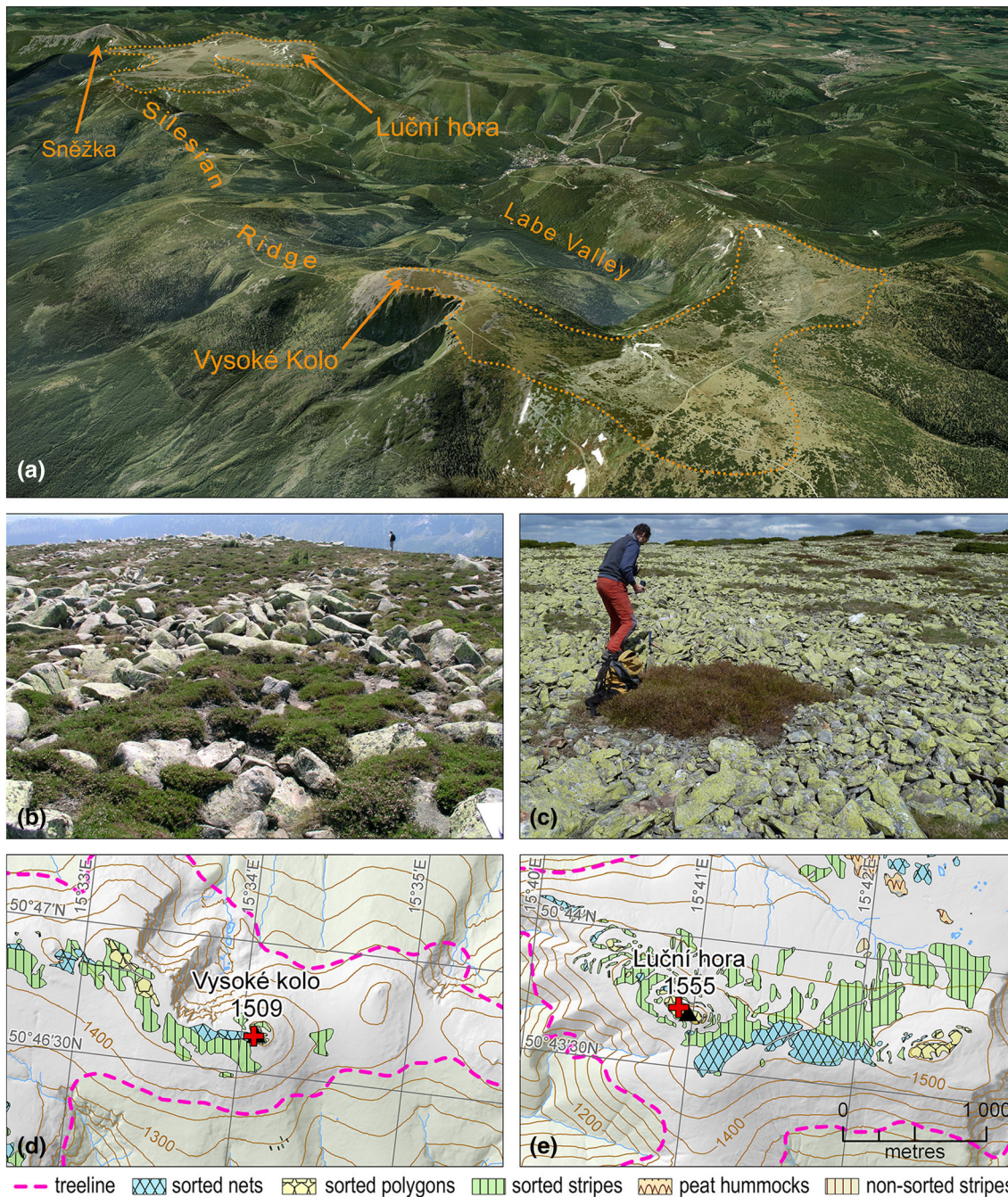


FIGURE 2 (a) The central part of the Krkonoše Mountains from the northwest with the location of the study sites. Sorted polygons on the summit of (b and d) Vysoké Kolo and (c and e) Luční hora Mountains. The red cross in (d) and (e) represents the location of sample sites and ERT profiles. Spatial distribution of patterned ground on the summit flats adopted from Krížek et al.⁴⁸

clinometer and a compass, and their location/altitude was determined using the global positioning system. The characteristics of the sampled boulders and study sites are presented in Tables 1 and 2, respectively.

3.2 | ¹⁰Be methodology

The samples were crushed, sieved, and cleaned with a mixture of HCl and H₂SiF₆. The extraction method for ¹⁰Be^{71,72} involves isolation

and purification of quartz and elimination of atmospheric ¹⁰Be. A weighed amount (~0.1 g) of a 3,025 ppm solution of ⁹Be was added to the decontaminated quartz. Beryllium was subsequently separated from the solution by successive anionic and cationic resin extraction and precipitation. The final precipitate was dried and heated at 800°C to obtain BeO and finally mixed with niobium powder prior to the measurements, which were performed at the French Accelerator Mass Spectrometry (AMS) National Facility ASTER (CEREGE, Aix en Provence).

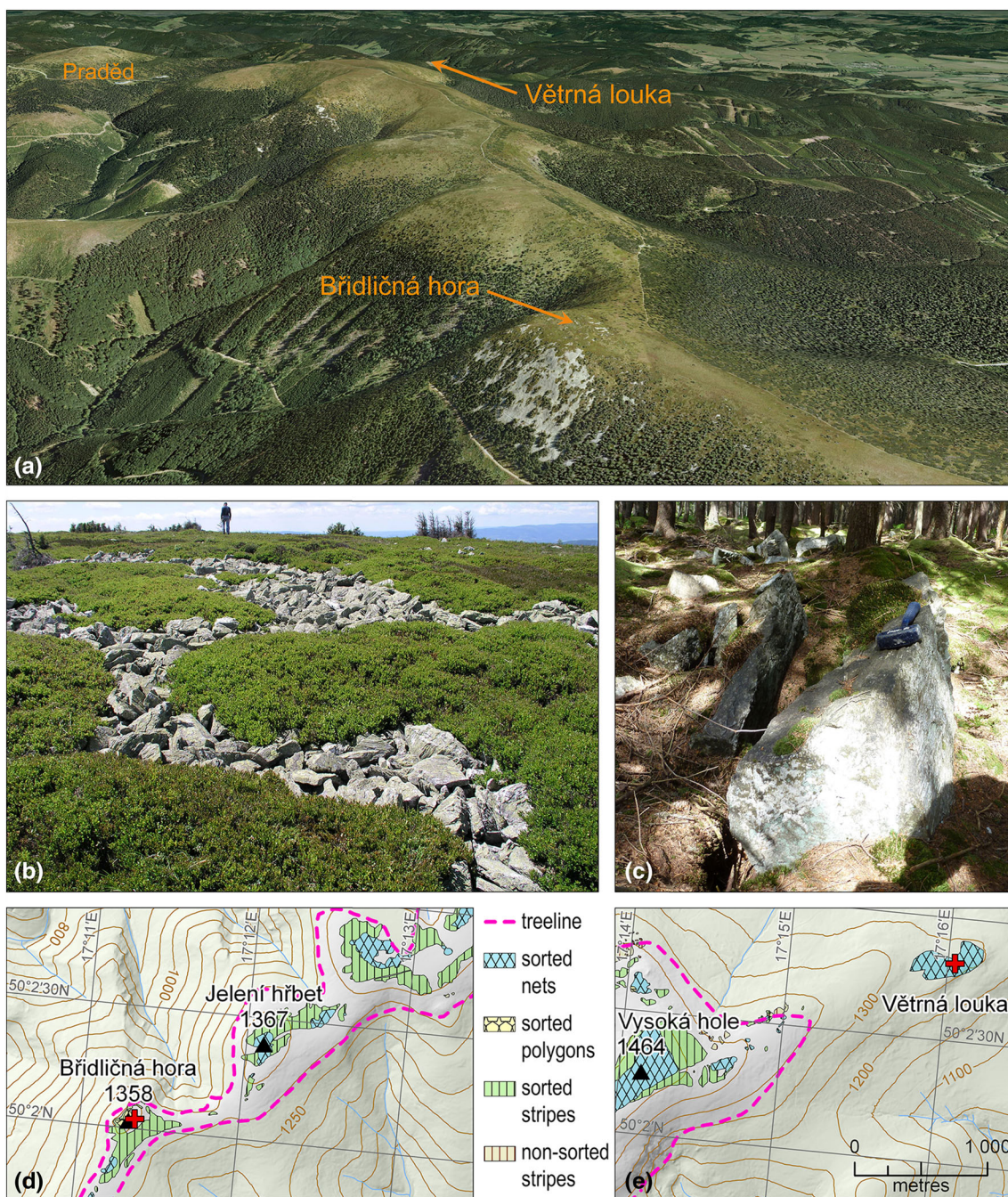


FIGURE 3 (a) The southern part of the Hrubý Jeseník Mountains from the southwest with the location of the study sites. Morphology and spatial distribution of patterned-ground landforms on (b and d) Břidličná hora and (c and e) Větrná louka

The beryllium data were calibrated directly against the STD-11 beryllium standard using a $^{10}\text{Be}/^9\text{Be}$ ratio of $1.191 \pm 0.013 \times 10^{-11.73}$. Age uncertainties include an external AMS uncertainty of 0.5%,⁷⁴ blank correction, and 1σ uncertainties. The $^{10}\text{Be}/^9\text{Be}$ measured blank ratio associated with the samples presented in this paper is 3.618×10^{-15} . A density of 2.5 g cm^{-3} was used for all samples. A sea-level, high-latitude spallation production of $4.01 \pm 0.18 \text{ g}^{-1} \text{ yr}^{-175}$ was used and scaled for latitude and elevation using Stone⁷⁶ scaling scheme. The surface production rates were also

corrected for the local slope and topographic shielding due to the surrounding terrain.⁷⁷ Shielding from snow was estimated using an average snow density of 0.3 g cm^{-3} and an estimated snow thickness and duration at sample sites.⁷⁸ These values were derived from the mean thickness and duration of snow cover during 1961–1990 at 14 weather stations (445–1,410 m a.s.l.) in the Sudetes Mountains. As the snow cover is unevenly distributed and its variation since the exposure of the sampled surfaces is unknown, the real effect of snow shielding remains uncertain. However, most of the samples were

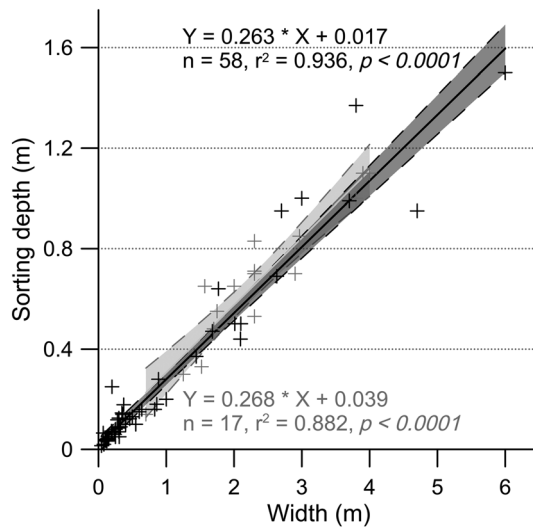


FIGURE 4 Width of sorted patterned ground used to estimate the active-layer thickness. Black crosses, solid lines, and dashed black lines indicate, respectively, the data (from references 5 and 51–66), linear fit, and 95% confidence intervals for active forms. Relict sorted polygons and circles (gray symbols; data from references 4, 9, 63, and 67) reveal a very similar relationship between width and sorting depth, confirming that these features indicate the active layer

extracted from windswept sites without vegetation, and we therefore suspect that temporal variation in snowfall has had a minor effect on snow conditions at these sites.

^{10}Be concentrations were modeled using the following equation:

$$C_{(x,\varepsilon,t)} = \frac{P_{\text{spall}}}{\Lambda_n + \lambda} \cdot e^{-\frac{x}{\Lambda_n}} \left[1 - \exp\left\{-t\left(\frac{\varepsilon}{\Lambda_n} + \lambda\right)\right\} \right] + \frac{P_{\mu}}{\Lambda_{\mu} + \lambda} \cdot e^{-\frac{x}{\Lambda_{\mu}}} \left[1 - \exp\left\{-t\left(\frac{\varepsilon}{\Lambda_{\mu}} + \lambda\right)\right\} \right] \quad (1)$$

where $C_{(x,\varepsilon,t)}$ is the nuclide concentration as a function of depth x (g cm^{-2}), ε is the denudation rate ($\text{g cm}^{-2} \text{ yr}^{-1}$), t is the exposure time (year), and λ is the radioactive decay constant (yr^{-1}). P_{spall} and P_{μ} are the relative production rates due to neutrons and muons, respectively. Λ_n and Λ_{μ} are the effective apparent attenuation lengths (g cm^{-2}) for neutrons and muons, respectively. The muon scheme follows Braucher et al.⁷⁹

3.3 | Data treatment

We assess the distribution of exposure ages obtained at individual sample sites, compare the arithmetic means and standard deviations (SDs) calculated for four age populations, and interpret the chronological data with exposure ages reported from the Sudetes Mountains in previous studies.

We first analyze the scatter in exposure-age data sets for each sample site because the age distribution reflects the exposure history of sampled surfaces and indicates the main sources of geological uncertainties—cosmogenic-nuclide inheritance and disturbance of

boulders after emplacement.⁸⁰ Among a group of samples, a sample with inherited ^{10}Be can be identified by a higher concentration that yields older age than the mean of the remaining ages. By contrast, a significant younger age may indicate incomplete exposure of the sampled boulder. The distribution of the exposure ages obtained for the given sample site and scatter in the age groups were approximated using the reduced chi-square statistics (χ_R^2) and SD to the arithmetic mean exposure age ratio. Following the procedure presented by Blomdin et al.,⁸¹ age groups that have $\chi_R^2 \leq 2$ are classified as well clustered, groups that show $\chi_R^2 > 2$ but $\text{SD} \leq 15\%$ of the mean exposure age are considered as moderately clustered, and groups that show $\chi_R^2 > 2$ and $\text{SD} > 15\%$ of the mean age are designated as poorly clustered.

Subsequently, we calculated an arithmetic mean and SD (1 s) for each site, compared these values, and assessed their relevance to the regional estimate of polygon chronology. When the age ranges of two or more sample sites overlap within their analytical uncertainties, we consider them representative of a regional interval of the sorted polygon formation. We compare this interval with regional glaciation chronology, and we interpret the data with respect to exposure ages reported for periglacial landforms in the Sudetes Mountains.^{82,83} An apparent age that differs significantly from the resulting age range is excluded from chronological consideration. A number of factors can cause apparent exposure ages of the sampled landforms, and these are discussed in Section 5.1.

4 | RESULTS

4.1 | Morphology of sorted polygons

The sorted polygons occur on flat or gently inclined surfaces (Figures 2b–e and 3b–e) with the median slope $\sim 3^\circ$ (Table 2). The length and width of the polygons range between 2.5–10.5 and 2.1–6.4 m, respectively (Table 3). The sorted polygons on VK have the largest average length (6.97 m), followed by the polygons on BR and VL, whereas the patterns with the smallest average length (3.67 m) lie on LH. The polygons on LH have significantly smaller width (Figure 5) than the polygons at other study sites (i.e., LH vs. VK: $F(1.41) = 26.643$, $p = 0.00001$; LH vs. BR: $F(1.62) = 19.491$, $p = 0.00004$; LH vs. VL: $F(1.38) = 14.576$, $p = 0.00048$). The sorted polygons with the largest average height lie on VL (Table 3; Figure 5), which significantly differs from other study sites (i.e., VL vs. LH: $F(1.38) = 260.24$; $p < 0.00001$; VL vs. VK: $F(1.17) = 71.698$, $p < 0.00001$; VL vs. BR: $F(1.38) = 201.41$; $p < 0.00001$).

4.2 | Regolith thickness

The high electrical-resistivity zones of more than $\sim 60,000 \Omega \text{ m}$ at the VK, LH, and BR sites (Figure 6a–c) are associated with the presence of air-filled debris. By contrast, the resistivity of the weathering mantle at VL is lower (Figure 6d) because this site lies below the alpine

TABLE 1 Morphological characteristics and ¹⁰Be surface exposure ages for sample boulders

Sample	Latitude °N	Longitude (°E)	Altitude (m a.s.l.)	Boulder l ength/width/ height (m)	Surface aspect/ dip (°)	Sample thickness (cm)	Snow depth/ duration (cm/month)	Total shielding factor	Production rate (at ⁻¹ g ⁻¹ yr ⁻¹)	¹⁰ Be concentration (at ⁻¹ g ⁻¹)	¹⁰ Be age (year)	Analytical uncertainty (±year)	Total uncertainty (±year)
VK-1	50.77646	15.56757	1,506	2.2/0.6/0.6	260/2	2	80/6	0.93035	12.93	377,555 ± 14,199	29,244	1,100	2,071
VK-2	50.77648	15.56754	1,503	1.3/0.3/0.5	320/5	5	80/6	0.93035	12.90	288,275 ± 10,354	22,342	802	1,562
VK-3	50.77652	15.56754	1,506	1.2/0.3/0.7	295/6	5	80/6	0.93035	12.93	242,577 ± 8,922	18,740	689	1,319
VK-4	50.77690	15.56740	1,507	1.1/0.3/0.3	330/10	3	80/6	0.93035	12.94	299,912 ± 10,732	23,177	829	1,619
VK-5	50.77691	15.56739	1,506	0.8/0.3/0.2	265/12	3	80/6	0.93035	12.93	367,295 ± 14,630	28,444	1,133	2,048
VK-6	50.77686	15.56731	1,507	1.5/0.3/0.2	120/7	6	80/6	0.93035	12.94	391,981 ± 14,423	30,347	1,117	2,136
LH-1	50.72779	15.68043	1,545	0.8/0.6/0.3	125/25	6	80/6	0.93034	13.32	1,195,921 ± 36,891	91,318	2,817	6,161
LH-2	50.72779	15.68046	1,544	0.8/0.5/0.2	0/0	6	80/6	0.93034	13.31	817,575 ± 33,737	62,023	2,559	4,517
LH-3	50.72780	15.68053	1,543	0.6/0.3/0.2	195/8	5	80/6	0.93034	13.30	824,325 ± 27,287	62,592	2,072	4,289
LH-4	50.72753	15.68201	1,549	0.9/0.5/0.6	325/3	4	80/6	0.93035	13.36	120,079 ± 74,821	8,955	5,580	5,606
LH-5	50.72751	15.68197	1,549	0.8/0.5/0.2	160/7	5	80/6	0.93035	13.36	480,431 ± 16,389	36,074	1,231	2,490
LH-6	50.72749	15.68203	1,546	0.9/0.6/0.3	110/5	3	80/6	0.93035	13.33	803,916 ± 30,423	60,876	2,304	4,318
BR-1	50.03324	17.18731	1,354	0.8/0.2/0.6	240/6	3	55/6	0.95101	12.01	455,811 ± 18,923	38,086	1,581	2,779
BR-2	50.03330	17.18732	1,355	1.4/0.4/0.5	0/0	4	55/6	0.95101	12.02	347,730 ± 12,938	28,967	1,078	2,045
BR-3	50.03324	17.18719	1,354	0.7/0.2/0.4	0/0	5	55/6	0.95101	12.01	272,835 ± 10,804	22,710	899	1,633
BR-4	50.03326	17.18737	1,354	0.6/0.2/0.5	0/0	7	55/6	0.95101	12.01	311,639 ± 13,077	25,961	1,089	1,901
BR-5	50.03327	17.18739	1,353	0.8/0.2/0.5	0/0	4	55/6	0.95101	12.00	347,506 ± 15,893	28,994	1,326	2,187
BR-6	50.03330	17.18739	1,354	0.6/0.1/0.4	0/0	7	55/6	0.95101	12.01	275,968 ± 11,455	22,972	954	1,676
VL-1	50.07115	17.26567	1,266	1.6/0.4/1.7	25/5	5	50/5	0.96271	11.46	234,005 ± 9,602	20,392	837	1,482
VL-2	50.07105	17.26560	1,267	1.1/0.5/0.7	0/0	5	50/5	0.96271	11.39	542,127 ± 15,768	47,868	1,392	3,192
VL-3	50.07115	17.26568	1,266	1.8/0.4/1.5	250/4	4	50/5	0.96271	11.33	201,218 ± 7,200	17,718	634	1,238
VL-4	50.07096	17.26572	1,266	1.9/0.3/0.9	145/12	6	50/5	0.96271	11.38	187,172 ± 7,019	16,411	615	1,161
VL-5	50.07095	17.26580	1,266	0.9/0.4/0.7	0/0	6	50/5	0.96271	11.39	270,860 ± 9,889	23,773	868	1,670
VL-6	50.07091	17.26584	1,266	0.9/0.2/0.6	30/12	6	50/5	0.96271	11.33	224,345 ± 8,523	19,764	751	1,404

Note. BR, Břídličná hora; LH, Luční hora; VK, Vysoké Kolo; VL, Větrná louka.

TABLE 2 Sample site characteristics and mean ¹⁰Be exposure ages for patterned ground in the Sudetes Mountains

Site	Altitude (m a.s.l.)	Mean/ median slope (°)	Elevation relative to local tree line (m)	Bedrock	Density (g cm ⁻³) ⁷⁰	Mean size of polygon boulders (m)	Montane ecosystem	Vegetation	χ^2_R	SD to mean exposure age (%)	Exposure age ± uncertainty (kyr)		
											Age clustering	Maximum	Mean
Vysoké Kolo	1,503–1,507	3/3	+128	Fine-grained biotite granite	2.69	0.85	Tundra	Grasses, lichens	30.7	18	Poorly clustered	30.3 ± 1.1	25.4 ± 1.9
Luční hora	1,543–1,549	3/2	+143	Quartzite	2.65	0.23	Tundra	Lichens	97.2	52	Poorly clustered	91.3 ± 2.8	53.6 ± 11.4
Břidličná hora	1,353–1,355	4/4	+30	Quartz-rich phyllite	2.73	0.75	Tundra	Grasses, lichens, and dwarf shrubs	21.4	20	Poorly clustered	38.1 ± 1.6	27.9 ± 2.3
Větrná louka	1,266–1,267	3/3	–87	Quartz-rich phyllite	2.73	1.17	Forest	Spruce forest	123.8	49	Poorly clustered	47.9 ± 1.4	24.3 ± 4.8

Note. SD, standard deviation.

timberline and is covered with a thick top-soil layer, which supports the cavities between the boulders with fine-grained materials. In addition, the quartzite vein crossing the VL site causes a slight bedrock protrusion, whereas at other locations the bedrock is mostly parallel to the ground surface. The regolith at the VK, BR, and VL sites is two to three times thicker than that at the LH site where regolith/bedrock transition is ~2 m (Figure 6b) below the ground surface. The small depth of bedrock at this site is constrained by the nearest cryoplanation terrace located 3 m lower.

4.3 | Exposure ages

For all studied sites, the surface exposure age is scattered (Table 1 and Figure 7), and age groups are poorly clustered (Table 2). The exposure ages obtained for the patterned ground on VK yield a mean age of 25.4 ± 1.9 ka and an oldest age of 30.3 ± 1.1 ka. This boulder group has the smallest scatter, and ages range from 19 to 30 ka. The boulder group from the sorted polygons on LH has a mean age of 53.6 ± 11.4 ka. The exposure ages from this summit flat show the largest scatter of all the study sites, ranging from 91.3 ± 2.8 to 9.0 ± 5.6 ka. The exposure ages obtained on BR yield a mean age of 28.0 ± 1.0 ka and a maximum age of 38.1 ± 1.6 ka. This oldest age is significantly older than the calculated mean age, but the remaining ages fall within a narrow range of 23–29 ka. The boulder group from VL has a mean exposure age of 24.3 ± 4.8 ka and an oldest age of 47.9 ± 1.4 ka, which is an obvious outlier according to the χ^2 criterion.

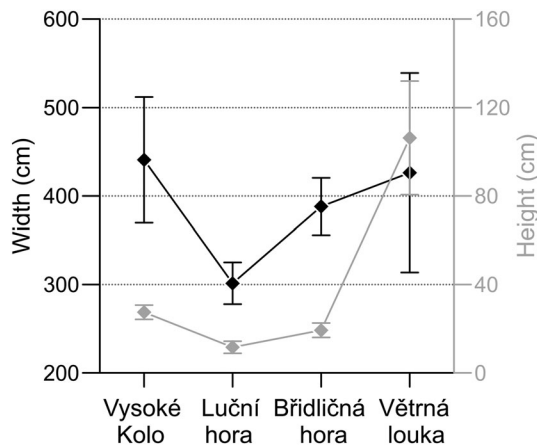
5 | DISCUSSION

5.1 | Exposure age interpretation and uncertainties

The scatter in age groups indicates that some sampled boulders experienced complex exposure history or post-exposure disturbance. An observed distribution of six exposure ages is affected by the presence of one or two apparently younger ages and one significantly older age than the mean age at all but one sample site. A significantly older sample age than the mean exposure age calculated for the landform results from cosmogenic-nuclide inheritance.⁸⁴ The most probable reason for the inherited nuclide concentration in boulders that form the margins of sorted polygons is their initial position at shallow subsurface depth affected by cosmic-ray flux. The cosmogenic-nuclide production decreases rapidly with depth, and it is largely attenuated below ~1 m depth.⁸⁵ The boulders located below the fine-grained regolith in this thin subsurface zone (Figure 8b) contain inherited ¹⁰Be from a period before the frost-heave event, and they will show apparently older age than boulders with zero inherited nuclide concentration frost heaved from greater depths. An alternative scenario that could lead to inheritance deals with the repeated phase of polygon formation and emplacement of

TABLE 3 Morphology of patterned ground at sample sites

Site	Altitude (m a.s.l.)	Mean length (m)	Mean width (m)	Mean height (m)	Width/length index	Minimum–maximum length	Minimum–maximum width	Minimum–maximum height	N
Vysoké Kolo	1,503–1,507	6.97	4.33	0.27	0.64	3.80–10.50	2.50–6.00	0.22–0.34	9
Luční hora	1,543–1,549	3.67	3.01	0.11	0.83	2.50–5.60	2.10–5.40	0.00–0.30	32
Břidličná hora	1,353–1,355	5.05	3.88	0.19	0.79	3.20–9.40	2.70–6.40	0.05–0.45	32
Větrná louka	1,266–1,267	4.76	4.26	1.06	0.91	2.50–6.80	2.30–6.00	0.50–1.50	8

**FIGURE 5** Differences in the mean width (black) and height (gray) of the sorted polygons at study sites. The error bars represent 95% confidence intervals

boulders that had experienced previous exposure at the margins of former polygons. However, this scenario is less probable as most of these boulders disintegrate over the period between two subsequent cold stages, and similar or higher freeze–thaw activity would be necessary to rearrange the existing polygons.

The presence of apparently younger boulders in the margins of sorted polygons could be attributed to post-exposure tilting of sampled surfaces⁸⁶ rather than to surface erosion or disintegration because only boulders without signs of erosion or fractures were sampled. The post-exposure shielding of sample sites by ice or snow cover can also be excluded from this consideration. Glaciers were confined to cirques and valleys during the LGM,⁸² and hypothetical plateau ice fields were suggested to cover high elevations except the wind-swept top of the ridges.⁸⁷ The presence of permanent snow cover is rather improbable because of reduced precipitation (25–75%) in cold stages^{35,88} and more effective deflation by enhanced winds.³⁴ Moreover, the effect of snow shielding would be rather uniform at each site without larger differences between individual boulders. Finally, the younger age of particular boulders cannot result from mass shielding by vegetation and/or soil cover that is evenly spread over the sample sites.

The obtained chronological data suggest that the large sorted polygons in the Sudetes Mountains developed during the last glacial period. Considering the relatively small areal extent of the Sudetes

Mountains, narrow elevation range of the sample sites, and similar topographic and climate conditions at these sites, it seems reasonable to expect the concurrent formation of these patterns throughout the Sudetes. However, the summed probability density distribution of all the obtained ¹⁰Be exposure ages is bimodal, with a main peak centered on 25 ka and a minor increase ~64 ka (Figure 7, black curve). The main peak indicates that the formation of sorted polygons started no later than 30 ka, reached a climax ~25 ka, and ceased after 18 ka. The second modeled peak reflects the high levels of *in situ*-produced ¹⁰Be in samples from the LH site. These samples seem to be affected by inheritance as indicated by apparently older mean age (53.6 ± 11.4 ka) compared to other sites (24.3 ± 4.8–27.9 ± 2.3 ka). The possible reasons for the inheritance are discussed. The reduced data set (n = 18) without exposure ages from LH yields the mean exposure age of 25.0 ± 0.4 ka (Figure 7, gray curve).

The largest scatter in the age group from LH confirms that inheritance must be considered at this site. The exposure age of 91.3 ± 2.8 ka is the oldest within the whole data set, and the apparent mean age is significantly older than the timing of the established main phase of polygon formation. The inheritance at this site may be tentatively attributed to the quartzite bedrock and poorly developed regolith cover. Despite the presence of surface features caused by differential weathering, the quartzite is more resistant to physical weathering and erosion than granite and phyllite at other sample sites. The hardness of the massive quartzite and considerably reduced surface lowering of landforms built by this rock were reported from many regions, including the Sudetes Mountains.^{32,90} The effect of the rock hardness on an exposure age was observed by Guido et al.,⁹¹ who reported a significantly older exposure age (30.2 ka) for a quartzite knoll compared to ages from other rock types (12.3–17.1 ka).

The hardness of the quartzite exerts control on the rate of weathering that is much lower compared to the weathering rate of granite and phyllite bedrock. As a result, a thin layer of regolith forms on LH where the bedrock lies only ~2 m below the ground surface. By contrast, 4–9 m of weathered rock covers the bedrock at the remaining study sites (Figure 6). The sorting depth corresponds to the thickness of the regolith cover ranging from less than 0.5 m on LH to ~1.4 m on BR.^{92,93} Considering the mean attenuation path length of neutrons in rocks⁸⁴ and the depth of boulders (>0.5 m) before the initiation of polygon formation on LH, the relatively small boulders at this site contain a substantial inherited nuclide component. By contrast, larger boulders that form polygons at other sites (Table 2) have

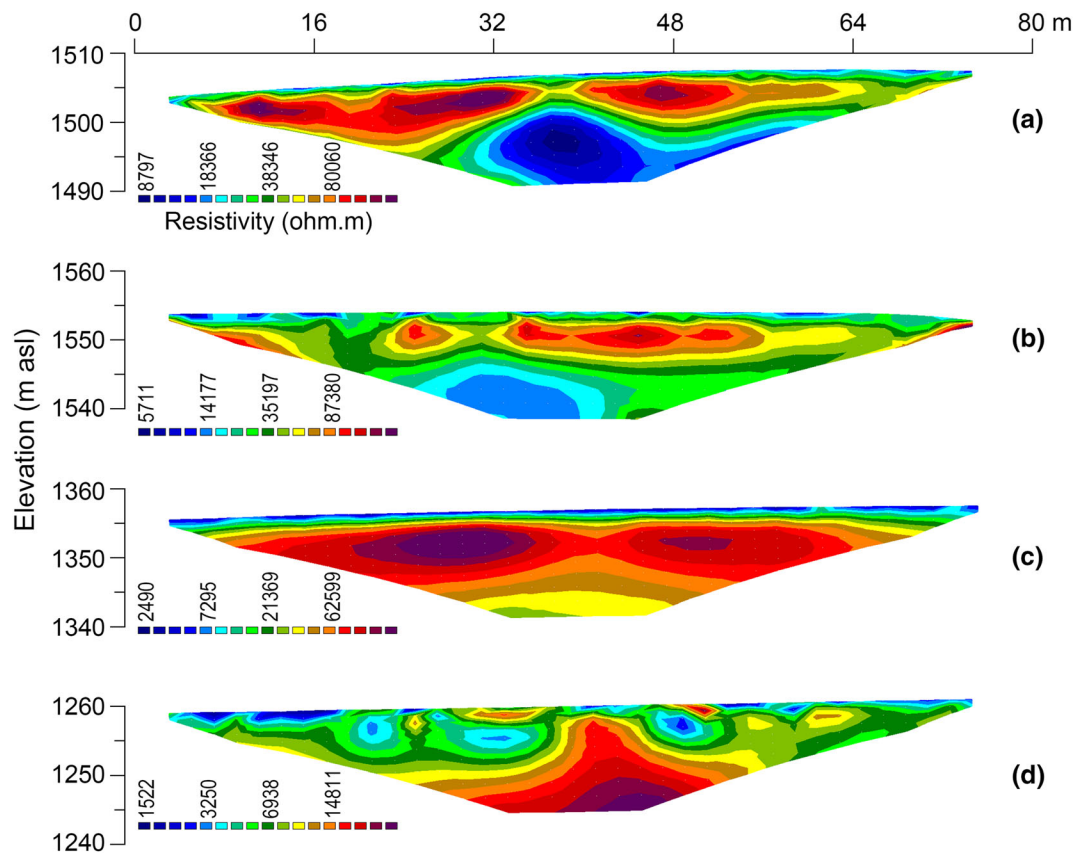


FIGURE 6 Resistivity tomograms performed on the summit of (a) Vysoké Kolo, (b) Luční hora, (c) Břidličná hora, and (d) Větrná louka. Electrode spacing is 2 m. The distances above each profile are in meters

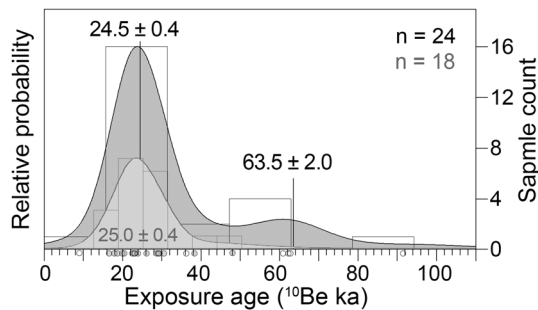


FIGURE 7 The probability distribution of ^{10}Be exposure ages obtained for all the samples (black curve with gray fill) and the data set without samples from Luční hora ($n = 18$; gray curve with light-gray fill). Thick curves mark kernel density estimation, and vertical lines indicate the mean ages with uncertainties for the modeled peaks

significantly less-inherited ^{10}Be as these were frost heaved from the depth of more than 1.4 m.

The high fraction of boulder ages with inheritance indicates that exposure dating should be applied on polygon boulders with caution. The age uncertainty resulting from the effects of vegetation and snow cover shielding seems to be of minor importance. All sample sites except VL are located above the timberline in the zone of limited vegetation and snow cover that is effectively transported

from the summit flats by the prevailing westerly winds.⁴² The timberline increased to its current position in the Sudetes Mountains during the early Holocene, and forest has covered the VL site at least over the past 8 ka.⁹⁴ Considering that boreal forest can reduce the cosmic-ray flux by $2.3 \pm 0.6\%$,⁹⁵ the estimated timing of polygons at this site could be underestimated only by a few hundred years.

5.2 | Paleoenvironmental implications

The exposure ages indicate that large sorted polygons in the Sudetes Mountains formed during the Upper Pleniglacial (34.8–14.7 ka)⁹⁶ after a period of unstable climate in the second part of MIS 3.^{97,98} The onset of the polygon formation corresponds to the Greenland sub-stadial GS-5.1 (30.6–28.9 ka),⁹⁹ and the main activity of these land-forms reflects extremely cold and relatively wet conditions in the Northern Hemisphere during the stadial GS-3 (27.5–23.3 ka).¹⁰⁰ The period of polygon formation overlaps with the range of 30–24 ka (Figure 9), which is considered as the period of the maximum extension of permafrost (Last Permafrost Maximum [LPM])¹⁰¹ in Western Europe during the last glacial cycle.¹⁰² The timing of the dated polygons is in line with the two (35–31 and 22–20 ka) of four main phases of periglacial activity in Britain lowlands,²² and corresponds to some

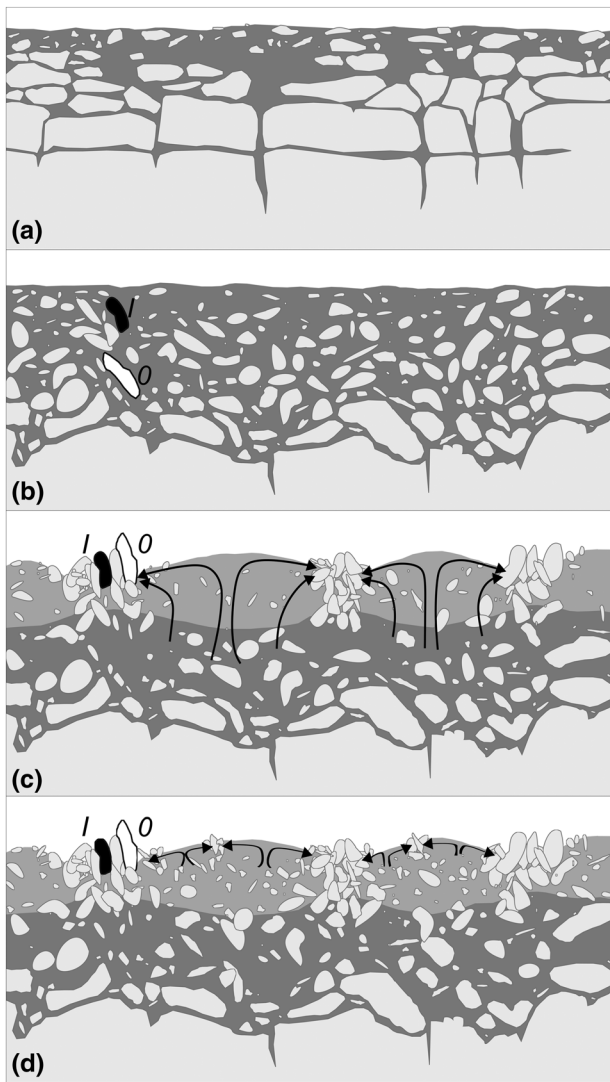


FIGURE 8 Concept of large sorted polygon formation: (a) regolith formation, (b) onset of differential frost heave and buoyancy-driven clast circulation, (c) well-developed forms composed of frost-heaved and laterally sorted boulders and finer clasts in the center,^{1,89} and (d) formation of small sorted patterns in the fine domain of a larger sorted polygon. Dark and light gray colors show a regolith matrix and the central fine domain of sorted polygons, respectively. I and O mark the location of boulders with inherited nuclide component and zero inheritance, respectively. Arrows indicate the motion of clasts within the fine domain

phases (30.0 ± 2.5 , 24.0 ± 1.1 , and 20.7 ± 0.7 ka) of ice-wedge activity in France.¹⁰²

The onset of differential frost heave in the Sudetes coincides with the pre-LGM period of periglacial conditions indicated recently by ¹⁰Be exposure ages (Figure 9). The exposure age of 36.5 ± 2.1 and 29.7 ± 2.1 ka reported for a summit tor and ploughing block, respectively, delimits the interval of bedrock disintegration and enhanced solifluction in the Krkonoše Mountains (Figure 9).⁸² Four exposure ages (84.3 ± 3.8 – 26.8 ± 2.6 ka) retrieved recently for a block slope adjacent to the VL site constrain the pre-LGM timing of cold

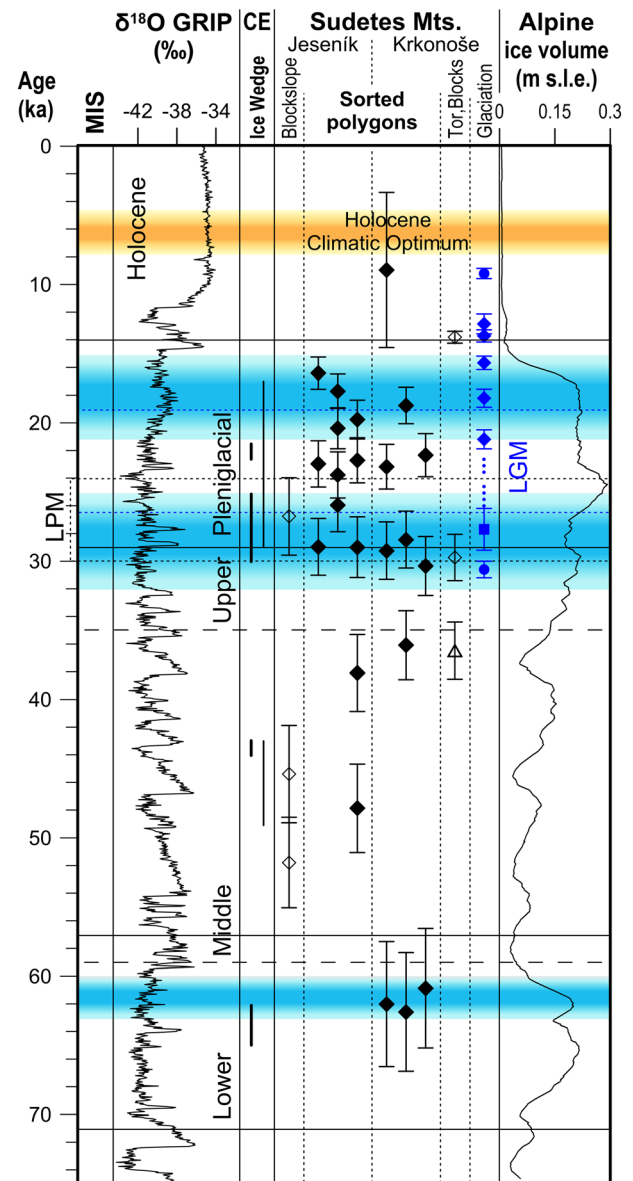


FIGURE 9 Age constraints for large sorted polygons in the Sudetes Mountains. Black diamonds with bars represent single ¹⁰Be exposure ages with total uncertainty ranges for the dated polygons. Unfilled black diamonds and triangles indicate ¹⁰Be timing for emplacement of blocks in slope cover deposits and tor surface, respectively.^{82,83} Blue diamonds show ¹⁰Be chronology of glacier advances in the Krkonoše Mountains, and blue dots indicate earlier advances poorly constrained with exposure ages.⁸² Blue circles and squares mark ice-free conditions in the upper Labe Valley in the Krkonoše dated by AMS ¹⁴C and optically stimulated luminescence, respectively.¹⁰³ Thick and thin black lines indicate periods of ice-wedge formation in the central European loess belt^{96,102} and forelands of the Sudetes Mountains,^{104,105} respectively. Modeled ice volume in the Alps is adopted from Seguinot et al.¹⁰⁰ The time scale on the left-hand side of the figure is based on the GICC05 data,^{99,106} MIS chronology after Lisiecki and Raymo,¹⁰⁷ chronostratigraphic units after Antoine et al.,⁹⁶ Last Permafrost Maximum after Andrieux et al.,¹⁰² and Last Glacial Maximum after Clark et al.¹⁰⁸ The shaded ochre area indicates the timing of the Holocene climatic optimum,¹⁰⁹ and the blue areas mark cold periods^{110,111} in the study area

environments in the Hrubý Jeseník Mountains.⁸³ At that time, permafrost reached its maximum extent and thickness (220–250 m) as indicated by the subsurface post-cryogenic structures near the eastern boundary of the Sudetes Mountains,¹¹² the model-based estimates,³⁴ and the cryogenic cave carbonates.¹¹³ The size of polygons dated in this study implies an active-layer thickness of 0.9–1.6 m. This range is consistent with the summer thawing to a depth of 1 m suggested by Jahn¹¹⁴ for LGM interval.

The occurrence of sorted polygons indicates cold conditions and lack of thick snow cover on the upper slopes of the Sudetes Mountains between 30 and 18 ka. Considering the most respected temperature threshold for the sorted polygon formation, the MAAT was lower than -4°C .⁹ The derived paleotemperature represents the maximal value for an elevation range of 1,210–1,270 m a.s.l. where dated polygons are preserved at the VL site. Assuming the near-surface lapse rate in the lower troposphere (0.65 K per 100 m), the MAAT on the summit flats $\sim 1,550$ m a.s.l. was probably lower than -6°C . The estimated temperature range is higher than the MAAT estimates for LGM that vary between -8 and -10°C .^{35,115} However, the paleotemperatures derived in this study must be regarded as maximal thresholds only because sorted polygons are also found at lower elevations within the Sudetes Mountains.

The regional warming of the climate after ~ 18 ka¹⁰³ led to the gradual degradation of permafrost in the Sudetes Mountains.³⁴ The intensity of frost action decreased allowing only for cryoturbation, solifluction, and limited sorting of fine-grained covers.¹¹⁶ The periglacial activity increased again at the end of the late glacial period when the climate cooled and permafrost re-aggraded.^{103,117} The exposure ages reported for moraines (13.5 ± 0.5 – 12.9 ± 0.7 ka) and pronival ramparts (13.8 ± 0.4 ka) in the Krkonoše Mountains indicate glacier readvance and enhanced frost action (Figure 9).⁸² At that time, frost sorting and solifluction were probably reactivated.¹¹⁷ Small sorted patterns observed in the large dated polygons on LH summit flat may be tentatively attributed to that period though their later formation cannot be excluded.⁴⁹ During the Holocene, the frost action has been limited to cryoturbation, solifluction, and sorting of sandy covers in deflation areas with thin snow cover.⁵⁰

6 | CONCLUSIONS

Surface exposure dating using cosmogenic ^{10}Be provides the first geochronological data for the sorted forms of patterned ground in Central Europe. ^{10}Be exposure ages from the large sorted polygons at four sites in the Sudetes Mountains imply that these periglacial features started to form no later than 30 ka and their activity decreased after 20 ka. The initiation of polygon formation is consistent with the most widespread events of thermal-contraction cracking during the LPM in Central Europe and with periods of enhanced periglacial activity in the lowlands of Britain and France. The main phase of formation falls within the global LGM, matches the period of maximum glaciation and continuous permafrost distribution in the European mountains,

and correlates with the period of intense periglacial activity in the surrounding lowland areas.

The samples collected from the sorted polygons provide large scatter in exposure ages and significant age uncertainty. This scatter may result from the incorporation of boulders that are affected by inheritance or disturbances after their active upfreezing/frost heaving. The morphological evaluation of individual polygons and their assemblages at the study site is highly advisable as its results would allow for sample collections from suitable boulders and landforms. Although this evaluation reduces the possibility of sampling-eroded or sampling-disturbed polygons, the complex history of earlier exposure and/or later reactivation cannot be fully excluded.

ACKNOWLEDGMENTS

This research was supported by the Czech Science Foundation (project number: 17-21612S). The administrations of the Krkonoše Mountains National Park and the Protected Landscape Area of Jeseníky are acknowledged for providing permissions to work in the protected areas. ASTER AMS National Facility (CEREGE, Aix-en-Provence) is supported by the INSU/CNRS and the ANR through the “Projets thématiques d'excellence” program for the “Equipements d'excellence” ASTER-CEREGE action, IRD. The authors are grateful for helpful and constructive comments from two anonymous referees.

DATA AVAILABILITY STATEMENT

The processed data are available from the corresponding author on reasonable request.

ORCID

Zbyněk Engel  <https://orcid.org/0000-0002-5209-7823>

Tomáš Uxa  <https://orcid.org/0000-0001-9911-6529>

REFERENCES

- Hallet B. Stone circles: form and soil kinematics. *Philos T R Soc A*. 2013;371:1-17.20120357.
- Ballantyne CK. Patterned ground. In: Elias SA, Mock CJ, eds. *Encyclopedia of Quaternary Science*. 2nd ed. Amsterdam: Elsevier; 2013: 452-463.
- Harris SA, Brouchkov A, Guodong C. *Geocryology: Characteristics and Use of Frozen Ground and Permafrost Landforms*. London: CRC Press; 2018.
- Grab S. Characteristics and paleoenvironmental significance of relict sorted patterned ground, Drakensberg plateau, southern Africa. *Quaternary Sci Rev*. 2002;21:1729-1744.
- Uxa T, Mida P, Křížek M. The effect of climate on morphology and development of sorted circles and polygons. *Permafrost Periglac*. 2017;28:663-674.
- Winkler S, Matthews JA, Mourne RW, Wilson P. Schmidt-hammer exposure ages from periglacial patterned ground (sorted circles) in Jotunheimen, Norway, and their interpretative problems. *Geogr Ann*. 2016;98:265-285.
- Matsuoka N. Climate and material controls on periglacial soil processes: towards improving periglacial climate indicators. *Quatern Res*. 2011;75:356-365.
- Goldthwait RP. Frost sorted patterned ground: a review. *Quatern Res*. 1976;6:27-35.

9. D'Amico ME, Pintaldi E, Catoni M, Freppaz M, Bonifacio E. Pleistocene periglacial imprinting on polygenetic soils and paleosols in the SW Italian Alps. *Catena*. 2019;174:269-284.
10. Van Vliet-Lanoë B. Patterned ground and climate change. In: Pokrovsky OS, ed. *Permafrost: distribution, composition and impacts on infrastructure and ecosystems*. New York, NY: Nova Science Publishers; 2014:67-106.
11. Matsuoka N, Abe M, Ijiri M. Differential frost heave and sorted patterned ground: field measurements and a laboratory experiment. *Geomorphology*. 2003;52:73-85.
12. Peterson RA, Krantz WB. Differential frost heave model for patterned ground formation: corroboration with observations along a north American arctic transect. *J Geophys Res-Biogeophys*. 2008;113:1-17.G03S04.
13. Kessler MA, Werner BT. Self-organization of sorted patterned ground. *Science*. 2003;299(5605):380-383.
14. Van Vliet-Lanoë B, Seppälä M. Stratigraphy, age and formation of peaty earth hummocks (pounus), Finnish Lapland. *Holocene*. 2002;12:187-199.
15. Kling J. Relict sorted patterned ground in Rostu, northernmost Sweden. *Geogr Ann*. 1996;78:61-72.
16. Cannone N, Guglielmin M, Gerdol R. Relationships between vegetation patterns and periglacial landforms in northwestern Svalbard. *Polar Biol*. 2004;27:562-571.
17. Jeong G. Radiocarbon ages of sorted circles on King George Island, South Shetland Islands, West Antarctica. *Antarct Sci*. 2006;18:265-270.
18. Bateman MD. Thermoluminescence dating of the British coversand deposits. *Quaternary Sci Rev*. 1995;14:791-798.
19. Bateman MD, Hitchens S, Murton JB, Lee JR, Gibbard PL. The evolution of periglacial patterned ground in East Anglia, UK. *J Quaternary Sci*. 2014;29:301-317.
20. Fábrián SÁ, Kovács J, Varga G, et al. Distribution of relict permafrost features in the Pannonian Basin, Hungary. *Boreas*. 2014;43:722-732.
21. Rittenour TM. Dates and rates of earth-surface processes revealed using luminescence dating. *Elements*. 2018;14:21-26.
22. Bateman MD. Luminescence dating of periglacial sediments and structures. *Boreas*. 2008;37:574-588.
23. Marchant DR, Lewis AR, Phillips WM, et al. Formation of patterned ground and sublimation till over Miocene glacier ice in Beacon Valley, southern Victoria land, Antarctica. *Geol Soc Am Bull*. 2002;114:718-730.
24. Levy J, Marchant D, Head J. Distribution and origin of patterned ground on Mullins Valley debris-covered glacier, Antarctica: the roles of ice flow and sublimation. *Antarct Sci*. 2006;18(3):385-397.
25. Winkler S, Matthews JA, Haselberger S, et al. Schmidt-hammer exposure-age dating (SHD) of sorted stripes on Juvflye, Jotunheimen (central South Norway): Morphodynamic and palaeoclimatic implications. *Geomorphology*. 2020;353:1-19.107014.
26. Ballantyne CK, Stone JO. Trilineas, blockfields and the vertical extent of the last ice sheet in southern Ireland. *Boreas*. 2015;44:277-287.
27. Andrés N, Gómez-Ortiz A, Fernández-Fernández JM, et al. Timing of deglaciation and rock glacier origin in the southeastern Pyrenees: a review and new data. *Boreas*. 2018;47:1050-1071.
28. Denn AR, Bierman PR, Zimmerman SRH, Caffee MW, Corbett LB, Kirby E. Cosmogenic nuclides indicate that boulder fields are dynamic, ancient, multigenerational features. *GSA Today*. 2018;28:4-10.
29. Migoń P, Lidmar-Bergström K. Weathering mantles and their significance for geomorphological evolution of central and northern Europe since the Mesozoic. *Earth Sci Rev*. 2001;56(1-4):285-324.
30. Högbom B. Über die geologische Bedeutung des Frostes. *Bull Geol Inst*. 1914;12:257-390.
31. Sekyra J, Kociánová M, Štursová H, Dvořák IJ, Svoboda M. Frost phenomena in relationship to mountain pine. *Opera Corcon*. 2002;39:69-114.
32. Traczyk A, Migoń P. Cold-climate landform patterns in the Sudetes. Effect of lithology, relief and glacial history. *Acta U Carol Geogr Suppl*. 2000;35:185-210.
33. Antoine P, Rousseau DR, Degeai JP, et al. High-resolution record of the environmental response to climatic variations during the last interglacial-glacial cycle in Central Europe: the loess-palaeosol sequence of Dolní Věstonice (Czech Republic). *Quaternary Sci Rev*. 2013;67:17-38.
34. Czudek T. *Vývoj relief České republiky v kvartéru*. Brno: Moravské zemské museum; 2005.
35. Heyman BM, Heyman J, Fickert T, Harbor JM. Paleo-climate of the central European uplands during the last glacial maximum based on glacier mass-balance modeling. *Quatern Res*. 2013;79:49-54.
36. Nývlt D, Engel Z, Tyráček J. Pleistocene glaciations of Czechia. In: Ehlers J, Gibbard PL, Hughes PD, eds. *Quaternary Glaciations - Extent and Chronology: A Closer Look*. Amsterdam: Elsevier; 2011:37-46.
37. Treml V, Migoń P. Controlling factors limiting timberline position and shifts in the Sudetes: a review. *Geogr Pol*. 2015;88:55-70.
38. Ehlers J, Gibbard PL, Hughes PD (Eds). *Quaternary Glaciations - Extent and Chronology: A Closer Look*. Amsterdam: Elsevier; 2011.
39. Halásová O, Hančarová E, Vašková I. Časová a prostorová variabilita vybraných klimatologických a hydrologických prvků na území Krkonoše za období 1961-2000. *Opera Corcon*. 2007;44:171-178.
40. Daniel M, Materna J, Honig V, et al. Vertical distribution of the tick *Ixodes ricinus* and tick-borne pathogens in the northern Moravian Mountains correlated with climate warming (Jeseníky Mts., Czech Republic). *Cent Eur J Public Health*. 2009;17:139-145.
41. Coufal L, Míková T, Langová P. *Meteorologická data na území ČR za období 1961-90*. Praha: Český hydrometeorologický ústav; 1992.
42. Spusta V, Spusta V, Kociánová M. Ukládání sněhu na závětrných svazích české strany Krkonoše (tundrová zóna). *Opera Corcon*. 2003;40:87-104.
43. Žák J, Verner K, Sláma J, Kachlík V, Chlupáčová M. Multistage magma emplacement and progressive strain accumulation in the shallow-level Krkonoše-Jizera plutonic complex, Bohemian Massif. *Tectonics*. 2013;32:1493-1512.
44. Pláček A, Migoń P, Żyszkowska W. Low-gradient surfaces in the Sudetes - insights from the digital elevation model. *Univ Ostrav Acta Fac Rerum Nat Geogr Geol*. 2007;237:94-110.
45. Danišik M, Migoń P, Kuhlemann J, Evans NJ, Dunkl I, Frisch W. Thermochronological constraints on the long-term erosional history of the Karkonosze Mts., Central Europe. *Geomorphology*. 2010;117:78-89.
46. Janoušek V, Aichler J, Hanžl P, et al. Constraining genesis and geotectonic setting of metavolcanic complexes: a multidisciplinary study of the Devonian Vrbno group (Hrubý Jeseník Mts., Czech Republic). *Int J Earth Sci*. 2014;103:455-483.
47. Křížek M. Periglacial Landforms of the Hrubý Jeseník Mountains. In: Pánek T, Hradecký J, eds. *Landscapes and Landforms of the Czech Republic*. Cham: Springer; 2016:277-289.
48. Křížek M, Krause D, Uxa T, Engel Z, Treml V, Traczyk A. Patterned ground above the alpine timberline in the high Sudetes, Central Europe. *J Maps*. 2019;15(2):563-569.
49. Křížek M, Uxa T. Morphology, sorting and microclimates of relict sorted polygons, Krkonoše Mountains, Czech Republic. *Permafrost Periglac*. 2013;24:313-321.
50. Treml V, Křížek M, Engel Z. Classification of patterned ground based on morphology and site characteristics: a case study from the high Sudetes, Central Europe. *Permafrost Periglac*. 2010;21:67-77.
51. Ballantyne CK, Harris C. *The Periglaciation of Great Britain*. Cambridge: Cambridge University Press; 1994.

52. Ballantyne CK, Matthews JA. The development of sorted circles on recently Deglaciated terrain, Jotunheimen, Norway. *Arctic Alpine Res.* 1982;14:341-354.
53. Cook JD. *Active and relict sorted circles, Jotunheimen, Norway: a study of the altitudinal zonation of periglacial processes*[dissertation]. Cardiff: University of Wales; 1989.
54. Ellenberg L. Rezente Periglazialerscheinungen auf Cheju Dô, Südkorea. *Geogr Helvetica.* 1976;31:69-74.
55. Freund R. Die Kleinformen der Frostmusterböden: Vergleich Arktis - Alpen - Tropisches Hochgebirge. *Geogr Helvetica.* 1971;26:142-147.
56. Furrer G. Die Strukturbodenformen der Alpen. *Geogr Helvetica.* 1955;10:193-213.
57. Gleason KJ, Krantz WB, Caine N, George JH, Gunn RD. Geometrical aspects of sorted patterned ground in recurrently frozen soil. *Science.* 1986;232(4747):216-220.
58. Grab SW. Annually re-forming miniature sorted patterned ground in the high Drakensberg, southern Africa. *Earth Surf Process Landf.* 1997;22:733-745.
59. Hallet B, Prestrud S. Dynamics of periglacial sorted circles in Western Spitsbergen. *Quatern Res.* 1986;26:81-99.
60. Holness SD. Sorted circles in the maritime Subantarctic, Marion Island. *Earth Surf Process Landf.* 2003;28:337-347.
61. Humlum O, Christiansen HH. Mountain climate and periglacial phenomena in the Faeroe Islands. *Permafrost Periglac.* 1998;9:189-211.
62. Kück KM. *Periglacial features in the vicinity of Tiffindell ski resort, North East Cape Drakensberg, South Africa, and their implications for the development of the resort* [dissertation]. Grahamstown: Rhodes University; 1996.
63. Ray RJ, Krantz WB, Caine TN, Gunn RD. A model for sorted patterned-ground regularity. *J Glaciol.* 1983;29:317-337.
64. Troll C. Strukturböden, Solifluktion und Frostklima der Erde. *Geol Rundsch.* 1944;34:545-694.
65. Wilson P. Small-scale patterned ground, Comeragh Mountains, Southeast Ireland. *Permafrost Periglac.* 1992;3:63-70.
66. Wilson P, Clark R. Development of miniature sorted patterned ground following soil erosion in East Falkland, South Atlantic. *Earth Surf Process Landf.* 1991;16:369-376.
67. Love A. Patterned Ground at Beartooth Butte and East Summit, Wyoming: Geometry, Analysis, and Origin. In: Carson RJ, DeSimone D, Leonard EM, eds. *Quaternary Geology of the Clarks Fork Region, Northwestern Wyoming and Adjacent Montana.* Claremont, CA: Keck Geology Consortium; 1995:113-116.
68. Milsom J. *Field Geophysics.* Chichester: Wiley; 2003.
69. Heyman J, Applegate PJ, Blomdin R, Gribenski N, Harbor JM, Stroeven AP. Boulder height e exposure age relationships from a global glacial ¹⁰Be compilation. *Quat Geochronol.* 2016;34:1-11.
70. Christensen NI, Mooney WD. Seismic velocity structure and composition of the continental crust: a global view. *J Geophys Res.* 1995; 100(B6):9761-9788.
71. Chmeleff J, von Blanckenburg F, Kossert K, Jakob D. Determination of the ¹⁰Be half-life by multicollector ICP-MS and liquid scintillation counting. *Nucl Instrum Meth B.* 2010;263:192-199.
72. Korschinek G, Bergmaier A, Faestermann T, et al. A new value for the half-life of ¹⁰Be by heavy-ion elastic recoil detection and liquid scintillation counting. *Nucl Instrum Meth B.* 2010;268:187-191.
73. Braucher R, Guillou V, Bourlès DL, et al. Preparation of ASTER in-house ¹⁰Be/⁹Be standard solutions. *Nucl Instrum Meth B.* 2015;361: 335-340.
74. Arnold M, Merchel S, Bourlès DL, et al. The French accelerator mass spectrometry facility ASTER: improved performance and developments. *Nucl Instrum Meth B.* 2010;268(11-12):1954-1959.
75. Borchers B, Marrero S, Balco G, et al. Geological calibration of spallation production rates in the CRONUS-earth project. *Quat Geochronol.* 2016;31:188-198.
76. Stone JO. Air pressure and cosmogenic isotope production. *J Geophys Res.* 2000;105:23753-23759.
77. Dunne J, Elmore D, Muzikar P. Scaling factors for the rates of production of cosmogenic nuclides for geometric shielding and attenuation at depth on sloped surfaces. *Geomorphology.* 1999;27: 3-11.
78. Gosse JC, Phillips FM. Terrestrial in situ cosmogenic nuclides: theory and application. *Quaternary Sci Rev.* 2001;20:1475-1560.
79. Braucher R, Merchel S, Borgomano J, Bourlès DL. Production of cosmogenic radionuclides at great depth: a multi element approach. *Earth Planet Sci Lett.* 2011;309:1-9.
80. Balco G. Glacier change and paleoclimate applications of cosmogenic-nuclide exposure dating. *Annu Rev Earth Planet Sci.* 2020;48:21-48.
81. Blomdin R, Stroeven AP, Harbor JM, et al. Evaluating the timing of former glacier expansions in the Tian Shan: a key step towards robust spatial correlations. *Quaternary Sci Rev.* 2016;153:78-96.
82. Engel Z, Braucher R, Traczyk A, et al. ¹⁰Be exposure age chronology of the last glaciation in the Krkonoše Mountains, Central Europe. *Geomorphology.* 2014;206:107-121.
83. Engel Z, Braucher R, AsterTeam. Origin and ¹⁰Be surface exposure dating of a coarse debris accumulation in the Hrubý Jeseník Mountains, Central Europe. *Geomorphology.* 2020;365:1-12.107292.
84. Dunai TJ. *Cosmogenic Nuclides.* Cambridge: Cambridge University Press; 2010.
85. Phillips WM. A review of cosmogenic nuclide surface exposure dating: new challenges for Scottish geomorphology. *Scott Geogr J.* 2001;117:1-15.
86. French H. *The Periglacial Environment.* 4th ed. Chichester: Wiley; 2018.
87. Sekyra J, Sekyra Z. Former existence of a plateau icefield in Bílá louka meadow, eastern Giant Mountains: hypothesis and evidence. *Opera Corcon.* 2002;39:35-43.
88. Ludwig P, Schaffernicht EJ, Shao Y, Pinto JG. Regional atmospheric circulation over Europe during the last glacial maximum and its links to precipitation. *J Geophys Res-Atmos.* 2016;121:2130-2145.
89. Kessler MA, Murray AB, Werner BT, Hallet B. A model for sorted circles as self-organized patterns. *J Geophys Res.* 2001;106(B7): 13287-13306.
90. Knotek Z. Geologie Jizerských hor. In: Karpaš R, ed. *Jizerské hory - O mapách, kamení a vodě.* Vol.555 Liberec: Knihy; 2009:104-141.
91. Guido ZS, Ward DJ, Anderson RS. Pacing the post-last glacial maximum demise of the Animas Valley glacier and the San Juan Mountain ice cap, Colorado. *Geology.* 2007;35:739-742.
92. Prosová M. Studie o periglaciálních zjevech v Hrubém Jeseníku. *Přírodovědecký sborník Ostravského Kraje.* 1954;15:1-15.
93. Sekyra J. *Působení mrazu na půdu - kryopedologie se zvláštním zřetelem k ČR.* Praha: Nakladatelství Československé Akademie Věd; 1960.
94. Tremli V, Jankovská V, Petr L. Holocene dynamics of the alpine timberline in the high Sudetes. *Biologia.* 2008;63:73-80.
95. Plug LJ, Gosse JC, McIntosh JJ, Bigley R. Attenuation of cosmic ray flux in temperate forest. *J Geophys Res.* 2007;112:1-9.F02022.
96. Antoine P, Coutard S, Guerin G, et al. Upper Pleistocene loess-palaeosol records from northern France in the European context: environmental background and dating of the middle Palaeolithic. *Quat Int.* 2016;411:4-24.
97. Moseley GE, Spötl C, Svensson A, Cheng H, Brandstätter S, Edwards RL. Multi-speleothem record reveals tightly coupled climate between Central Europe and Greenland during marine isotope stage 3. *Geology.* 2014;42:1043-1046.
98. Agosta EA, Compagnucci RH. Abrupt Climate Changes During the Marine Isotope Stage 3 (MIS 3). In: Gasparini G, Rabassa J, Deschamps C, Tonni E, eds. *Marine Isotope Stage 3 in Southern South America, 60 ka B.P. - 30 ka B.P.* Cham: Springer; 2016:81-106.

99. Rasmussen SO, Bigler M, Blockley S, et al. A stratigraphic framework for abrupt climatic changes during the last glacial period based on three synchronized Greenland ice-core records: refining and extending the INTIMATE event stratigraphy. *Quaternary Sci Rev.* 2014; 106:14-28.
100. Seguinot J, Jouvet G, Huss M, Funk M, Ivy-Ochs S, Preusser F. Modelling last glacial cycle ice dynamics in the Alps. *Cryosphere.* 2018;12:3265-3285.
101. Vandenberghe J, French HM, Gorbunov A, et al. The last permafrost maximum (LPM) map of the northern hemisphere: permafrost extent and mean annual air temperatures, 25–17 ka BP. *Boreas.* 2014;43: 652-666.
102. Andrieux E, Bateman M, Bertran P. The chronology of Late Pleistocene thermal contraction cracking derived from sand wedge OSL dating in central and southern France. *Global Planet Change.* 2018; 162:84-100.
103. Engel Z, Nývlt D, Křížek M, Treml V, Jankovská V, Lisá L. Sedimentary evidence of landscape and climate history since the end of MIS 3 in the Krkonoše Mountains, Czech Republic. *Quaternary Sci Rev.* 2010;29:913-927.
104. Woronko B, Zielinski P, Sokołowski RJ. Climate evolution during the Pleniglacial and late glacial as recorded in quartz grain morphoscopy of fluvial to aeolian successions of the European Sand Belt. *Geologos.* 2015;21:89-103.
105. Kovács J, Moravcová M, Újvári G, Pintér AG. Reconstructing the paleoenvironment of east Central Europe in the Late Pleistocene using the oxygen and carbon isotopic signal of tooth in large mammal remains. *Quat Int.* 2012;276-277:145-154.
106. Lowe JJ, Rasmussen SO, Björck S, et al. Synchronisation of palaeoenvironmental events in the North Atlantic region during the last termination: a revised protocol recommended by the INTIMATE group. *Quaternary Sci Rev.* 2008;27:6-17.
107. Lisiecki LE, Raymo MR. A Pliocene-Pleistocene stack of 57 globally distributed benthic $\delta^{18}O$ records. *Paleoceanography.* 2005;20:1-17. PA1003.
108. Clark PU, Dyke AS, Shakun JD, et al. The last glacial maximum. *Science.* 2009;325(5941):710-713.
109. Juříčková L, Ložek V, Horáčková J, Tlachač P, Horáček I. Holocene succession and biogeographical importance of mollusc fauna in the Western Sudetes (Czech Republic). *Quat Int.* 2014;353:210-224.
110. Alexandrowicz WP, Ciszek D, Gołas-Siarzewska M. Malacological characteristic of the Weichselian upper Pleniglacial (MIS-2) loess profile in Tłumaczów (SW Poland). *Geol Q.* 2013;57(3):433-442.
111. Feurdean A, Perşoiu A, Tanţău I, et al. Climate variability and associated vegetation response throughout central and Eastern Europe (CEE) between 60 and 8 ka. *Quaternary Sci Rev.* 2014;106:206-224.
112. Růžičková E, Zeman A. The Blahutovice-1 borehole near Hranice na Moravě: weathering effects in Badenian deposits. *Scripta Fac Sci Nat Univ Masaryk Brun Geol.* 1992;22:128-132.
113. Žák K, Richter DK, Filippi M, et al. Coarsely crystalline cryogenic cave carbonate – a new archive to estimate the last glacial minimum permafrost depth in Central Europe. *Clim Past.* 2012;8:1821-1837.
114. Jahn A. The permafrost active layer in the Sudety Mountains during the last glaciation. *Quaest Geogr.* 1977;4:29-42.
115. Chmal H, Traczyk A. Plejstocénskie lodowce gruzowe w Karkonoszach. *Czas Geogr.* 1993;64(3-4):253-262.
116. Waroszewski J, Kalinski K, Malkiewicz M, Mazurek R, Kozłowski G, Kabala C. Pleistocene–Holocene cover-beds on granite regolith as parent material for Podzols—an example from the Sudeten Mountains. *Catena.* 2013;104:161-173.
117. Traczyk A. Late Pleistocene evolution of periglacial and glacial relief in the Karkonosze Mountains. New hypotheses and research perspectives. *Acta U Carol Geogr.* 2004;39:59-72.

How to cite this article: Engel Z, Křížek M, Braucher R, Uxa T, Krause D, AsterTeam. ^{10}Be exposure age for sorted polygons in the Sudetes Mountains. *Permafrost and Periglacial Process.* 2020;1-15. <https://doi.org/10.1002/ppp.2091>